NASA Technical Memorandum 4143

Nuclear-Fragmentation Studies for Microelectronic Applications

Duc M. Ngo, John W. Wilson,
Warren W. Buck, and Thomas N. Fogarty

NOVEMBER 1989

NASA

NASA Technical Memorandum 4143

Nuclear-Fragmentation Studies for Microelectronic Applications

Duc M. Ngo
Hampton University
Hampton, Virginia

John W. Wilson
Langley Research Center
Hampton, Virginia

Warren W. Buck and Thomas N. Fogarty
Hampton University
Hampton, Virginia

National Aeronautics and
Space Administration
Office of Management
Scientific and Technical
Information Division

1989

Abstract

A formalism for target fragment transport is presented with application to energy-loss spectra in thin silicon devices. Predicted results are compared with experiments using the surface-barrier detectors developed by J. P. McNulty. The intranuclear-cascade, nuclear-reaction model does not predict the McNulty experimental data for the highest energy events. A semiempirical nuclear cross section gives an adequate explanation of McNulty's experiments. Application of the formalism to specific electronic devices is discussed.

Introduction

The early suggestion that some spacecraft anomalies may result from the passage of the galactic ions through microelectronic circuits (ref. 1) has now been well established. Although the direct ionization by protons appears as an unlikely candidate, the recoil energy of nuclear-reaction products is a suspected as a source of single-event upset (SEU) phenomena (refs. 2 to 4). As a result, a number of fundamental experimental and theoretical studies were undertaken to better understand the phenomena. McNulty and coworkers examined the energy deposition of proton reaction products in Si using surface-barrier detectors of various thicknesses from 2.5 to 200 μm (ref. 5). They also developed a Monte Carlo code for theoretical evaluation of energy deposition from such products. (See refs. 5 and 6.) A comparison of McNulty's work with the well-established medium energy cascade code (MECC-7) developed by Bertini and coworkers at Oak Ridge National Laboratory showed some differences in predicted reaction products and even greater differences in energy spectral contribution. (See ref. 7.) An evaluation of Si reaction products was likewise made by Petersen (ref. 4), and, although no direct comparison was made with McNulty's experiments, an estimate of SEU rates in the trapped-proton environment was made.

Following these fundamental studies were more detailed applications to specific-device geometries and parameters. Bradford evolved an energy deposition formalism (ref. 8) using the cross sections of Hamm et al. (ref. 7). McNulty et al. (ref. 5) applied their Monte Carlo model to dynamic random access memory (DRAM) devices with reasonable success and discussed the implications of heavy-ion SEU phenomena on proton-induced SEU events through secondary reaction processes (ref. 9). The fundamental consideration is the evaluation of the energy deposited within the sensitive volume (depletion region) of the device in question as the result of a passing proton. The ionization due to the proton itself makes only a small contribution to the critical charge. Nuclear-reaction events usually produce several reaction products (a heavy fragment and several lighter particles, although a few heavy fragments may be produced simultaneously on some occasions), and all the resultant products can make important contributions to the deposited energy. Such nuclear-event products are, of course, correlated in both time and space.

There are three distinct approaches to a fundamental description of the energy deposition events. McNulty and coworkers developed a Monte Carlo code in which multiparticle events are calculated explicitly, including spatial and specific-event (temporal) correlation effects. Although this is the most straightforward way of treating the full detail, it is a complex computational task. A second class of methods begins with the volumetric source of collision events and calculates the SEU probability using the chord-length distribution. (See refs. 8 and 10.) Although in principle the correlation effects could be so incorporated, they appear to be ignored in both the cited references. A third approach in which linear energy transfer (LET) distributions and chord-length distributions are used seems most appropriate for external sources. (See refs. 11 and 12.) This last approach applies if the LET distribution from external sources is constant over the sensitive volume, but its applicability to volumetric sources is questionable. At the very least, this approach ignores correlation effects.

Nuclear data bases for biological systems were examined in reference 13. The MECC-7 results underestimated by nearly a factor of 2 the energy-transfer cross section for multiple-charged ion products. In a more detailed analysis (ref. 14), the Silberberg-Tsao fragmentation parameters were found to be superior to the MECC-7 results. The primary differences appear for the lighter of the multiple-charged fragments. Further comparison with experiments on Al targets shows both Monte Carlo nuclear models (McNulty's code OMNI as well as MECC-7) to underestimate production cross sections for products lighter than fluorine in proton-induced reactions. Although these intranuclear-cascade models are capable of representing multiparticle correlation, the inherent inaccuracies in predicting cross sections is a serious limitation.

In the present paper, the effects of nuclear recoil on electronic devices are examined and the development of a formalism for application to specific-device parameters is begun. As a test of our methods as they develop, the results are compared with the experimental measurements of McNulty et al. (ref. 5).

Symbols

A	atomic mass, amu
A_F	fragment atomic mass, amu
CMOS	complementary metal-oxide semiconductor
$\frac{dF}{d\epsilon}$	total absorption spectrum, MeV^{-1}
$\frac{d\sigma}{dA}$	cross section, mb
E_O	average fragment energy, MeV
F_z	inward-directed flux at boundary of type-z ions
$f(E_O)$	spectrum average energy, MeV
I^2L	integrate-integrate logic
L	feature size, μm
MECC-7	medium energy cascade code
NMOS	N-channel metal-oxide semiconductor
OMNI	McNulty code
PMOS	P-channel metal-oxide semiconductor
$P(E)$	energy-loss spectrum, MeV
Q_c	critical charge, pC
SOS	silicon on sapphire
Z	charge number
ϵ	energy loss, MeV
σ_F	nuclear fragment cross section, mb

Microelectronic Upsets

An electronic device is sensitive to the sudden introduction of charge into the active elements of its circuits. The amount of such charge that is sufficient to change state in a logic circuit is called the critical charge. As shown in figure 1, there is a rough relationship between the critical charge Q_c and the device feature size L (ref. 11). This relationship is as follows:

$$Q_c \approx 0.0156L^2 \tag{1}$$

where Q_c is measured in pC and L is measured in μm. Upsets in a device are then dependent on the charge produced in comparison to the critical charge.

The charge released ΔQ in a material because of the passage of an energetic ion is related to the kinetic energy lost ΔE during the passage and is given by

$$\Delta Q = \frac{\Delta E}{22.5} \tag{2}$$

where ΔQ has units pC and ΔE has units MeV. The energy lost by an ion in passing through a region is related to its stopping power $\left(-\frac{dE}{dx} = S_z(E')\right)$ in the medium. The distance traveled before coming to rest is

$$R_Z(E) = \int_0^E \frac{dE'}{S_z(E')} \tag{3}$$

If an ion is known to come to rest in distance x, then its energy is found through the inverse of relation (3) as

$$E = R_Z^{-1}(x) \tag{4}$$

Equation (4) is used to calculate energy loss. The energy loss by an ion of charge Z and energy E in passing through the active region of a device with collection length L_c is given by

$$\Delta E = E - R_Z^{-1}[R_Z(E) - L_c] \tag{5}$$

where

$$L_c = W_{\text{epi}} + W_n \tag{6}$$

In equation (6), W_{epi} is the epitaxial layer thickness and W_n is the width of the depletion region (ref. 15). The energy loss depends on the particle isotope (i.e., ion mass) and angle of incidence. The range-energy relations described in reference 14 are utilized. As a practical matter to reduce numerical error inherent to numerical interpolation,

$$\Delta E = R_Z^{-1}[R_Z(E)] - R_Z^{-1}[R_Z(E) - L_c] \tag{7}$$

is used in place of equation (5). The result of equation (5) depends on the global error (fixed at 1 percent) in the computer code, while equation (7) depends only on the local relative error (quite small). The charge introduced into the feature is given by equations (2) and (7). An example for a particular collection length of 2 μm is shown in figure 2 for each ion type. A simplified geometry is assumed in which the channel length and width and the collection length (fig. 3) are taken as equal to the feature size. The E, Z plane can be divided into regions for which

$$\Delta Q(E) \geq Q_c \tag{8}$$

The value of $\Delta Q(E)$ depends on the feature size L. (See eq. (1).) The ion mass for each value of Z was taken as the natural mass in arriving at the contour of constant ΔQ shown in figure 4. The average recoil energies from the fragmentation of ^{16}O and ^{28}Si produced by collision with high-energy protons (ref. 14) are also shown in figure 4. The importance of a given fragment type for a given feature size for the device may be judged from the average recoil energies from the fragmentation of ^{16}O and ^{28}Si.

It is doubtful that any of the fragments produce upsets in the 4-μm and larger devices (note that simplified geometries have been used). Also, the lighter fragments of Li, He, and H are not suspected for SEU events in this simple geometry and figure 4 is applicable to incident cosmic-ray ions.

Nuclear-Fragmentation Cross Section

Although nuclear fragmentation has been under study for nearly 50 years, the absolute cross sections still stir some controversy. The experimental problem was that the main-reaction products could be directly observed only in recent years and even now only in rather sophisticated experiments. Rudstam (ref. 16) studied the systematics of nuclear fragmentation and supposed the fragment isotopes to be in a bell-shaped distribution about the nuclear stability line. Silberberg and Tsao (ref. 12) continued the Rudstam parametric approach and added many correction factors as new experimental evidence became available.

Concurrently, Monte Carlo simulation of the Serber model (ref. 17) and final decay through compound nuclear models showed some success (refs. 7 and 18). Even so, Monte Carlo simulation shows little success in predicting fragments whose mass is small compared with the original target nuclear mass (refs. 13 and 19). Of the various models for nucleon-induced fragmentation in ^{28}Si, the model of Silberberg and Tsao (ref. 12) is probably the most reliable. The main limitation of their model is that only inclusive cross sections are predicted; particle correlations could prove important in predicting SEU.

Measurements of ^{27}Al fragmentation in proton beams have been made by Kwiatkowski et al. (ref. 19). These experiments are compared in figure 5 with the Monte Carlo results of OMNI and MECC-7. Also shown are the results from reference 16; generally, these results appear to be within a factor of 2 of the experiment. The model in reference 12 is the only model which predicts significant contributions in the important range below $A = 12$.

The spectrum of average recoil energy is calculated using the formalism of reference 14 and the Silberberg-Tsao cross sections and is shown for comparison with the spectrum according to the Bertini cross sections in figure 6. The Bertini cross sections are greatly underestimated above 8 MeV and greatly overestimated below 3 MeV. The Bertini results are typical for currently available intranuclear-cascade models. Experimental evidence indicates that even the Silberberg-Tsao values are too small above 6 MeV (ref. 19).

Nuclear Recoil Transport

The transport of the recoil fragments is described as follows:

$$\left[\Omega \cdot \nabla - \frac{\partial}{\partial E} S_z(E)\right] \phi_z(x, \Omega, E) = \zeta_z(E) \qquad (9)$$

where $\phi_z(x, \Omega, E)$ is the ion flux at x moving in direction Ω with energy E and where $\zeta_z(E)$ is the ion-source density assumed to be isotropic and uniformly distributed through the media. The solution to equation (9) is in a closed region bounded by the surface Γ subject to the boundary condition

$$\phi_z(\Gamma, \Omega, E) = F_z(\Omega, E) \qquad (n \cdot \Omega < 0) \qquad (10)$$

where n is the outward-directed normal of the surface Γ. The solution is found by using the method of characteristics (refs. 20 and 21) as

$$\phi_z(x, \Omega, E) = \frac{S_z(E_b)}{S_z(E)} \phi_z(\Gamma, \Omega, E_b) + \frac{1}{S_z(E)} \int_E^{E_b} \zeta_z(E')\, dE' \qquad (11)$$

where Γ is the point on the boundary determined by projecting x along in direction Ω and

$$E_b = R_Z^{-1}[R_Z(E) + b] \qquad (12)$$

where

$$b = \Omega \cdot (x - \Gamma) \qquad (13)$$

Equation (11) may be used to evaluate the spectrum of particles leaving the region that can be related to the spectrum of energy deposited in the media. An isolated sheet of silicon of thickness a, which is obviously similar to the McNulty surface-barrier detectors, is considered. The inward-directed flux at the boundary is then zero. We first consider a monoenergetic ion source

$$\zeta_z(E) = \frac{\sigma_z \phi}{4\pi} \delta(E - E') \qquad (14)$$

for which

$$\phi_z(x, \Omega, E) = \frac{\sigma_z \phi}{4\pi S_z(E)} \begin{cases} 1 & (E \le E' \le E_b) \\ 0 & (\text{Otherwise}) \end{cases} \qquad (15)$$

where σ_z is the silicon-fragmentation cross section and ϕ is the flux of initiating energetic particles. The spectrum of ions leaving the sheet (ignoring edge effects) is

$$\frac{df_z}{dE} = 4\pi A \int_0^1 \mu\phi_z(\Gamma, \Omega, E)\, d\mu$$

$$= \frac{A\sigma_z\phi}{2S_z(E)} \left\{ \begin{array}{cc} \frac{a^2}{[R_Z(E')-R_Z(E)]^2} & (0 \le E \le R_Z^{-1}\left[R_Z(E'-a]\right) \\ 1 & (R_Z^{-1}[R_Z(E')-a] \le E \le E') \\ 0 & (E' < E) \end{array} \right\} \tag{16}$$

where A is the area of the sheet and μ is the cosine of the colatitude with respect to the local surface normal. The total number of escaping particles is found by integrating the spectrum given by equation (16) and is

$$N_e = Aa\sigma_z\phi \left\{ \begin{array}{cc} \left[1 - \frac{a}{2R_Z(E')}\right] & (a \le R_Z(E')) \\ \frac{R_Z(E')}{2a} & (a > R_Z(E'')) \end{array} \right\} \tag{17}$$

From equation (17), the total number of ions which stop in the sheet is

$$N_S = Aa\sigma_z\phi \left\{ \begin{array}{cc} \left[\frac{a}{2R_Z(E')}\right] & (a \le R_Z(E')) \\ \left[1 - \frac{R_Z(E')}{2a}\right] & (a > R_Z(E')) \end{array} \right\} \tag{18}$$

Obviously, an ion produced with energy E' which leaves the sheet with energy E suffered an energy loss ϵ to the sheet given by

$$\epsilon = E' - E \tag{19}$$

which we use to find the energy-loss spectrum as

$$\frac{df_{z\delta}}{d\epsilon} = \left.\frac{df_z}{dE}\right|_{E=E'-\epsilon} + N_S\delta(E' - \epsilon) \tag{20}$$

Considering that equation (20) is the energy deposition in a sheet of area A and thickness a as the result of a monoenergetic volumetric source, the response to any arbitrary spectral source can be found by superposition.

Fragmentation Energy-Loss Spectra

The fragmentation-source energy distribution (normalized to unity) is given as

$$\rho(E') = \sqrt{\frac{E'}{2\pi E_O^3}} \exp\left(\frac{-E'}{2E_O}\right) \tag{21}$$

where $3E_O$ is the mean-fragment energy and is given by Wilson et al. (ref. 14) based on previous work by Goldhaber (ref. 22).

The energy-loss spectrum is found by using equations (20) and (21) as

$$\frac{dF}{d\epsilon} = \int_{\epsilon}^{\infty} \left.\frac{df_{z\delta}}{d\epsilon}\right|_{E=E'-\epsilon} \rho(E')\, dE'$$

$$= \int_{0}^{\infty} \left.\frac{df_{z\delta}}{d\epsilon}\right|_{E=E'+\epsilon} \rho(E+\epsilon)\, dE \tag{22}$$

The contribution from stopping ions is readily evaluated to give

$$\frac{dF}{d\epsilon} = N_S(\epsilon)\rho(\epsilon) + \int_{0}^{\infty} \left.\frac{df_{z\delta}}{d\epsilon}\right|_{E'=E+\epsilon} \rho(E+\epsilon)\, dE \tag{23}$$

where the second term of equation (23) requires more attention.

The energy-degradation function in the integral of equation (23) is given by equation (16). It is not clear how the integral in equation (23) is to be evaluated. As an approximate evaluation, the energy-degradation function is approximated by two or three line segments as shown in equations (24) to (27).

If $R_Z(\epsilon) > 2a$, then

$$\left.\frac{df_z}{dE}\right|_{E'=E+\epsilon} = \frac{A\sigma_z\phi}{2S_z(E)} \left\{ \begin{array}{cc} \frac{a^2}{R_Z^2(\epsilon)} + \left[\frac{1}{4} - \frac{a^2}{R_Z^2(\epsilon)}\right] \frac{R_Z(E)}{R_Z(E_2)} & (0 \le E \le E_2) \\ \frac{1}{4} + \frac{3[R_Z(E)-R_Z(E_2)]}{4[R_Z(E_1)-R_Z(E_2)]} & (E_2 \le E \le E_1) \\ 1 & (E_1 \le E \le \infty) \end{array} \right\} \tag{24}$$

where E_2 is the solution of

$$R_Z(E_2) = R_Z(E_2+\epsilon) - 2a \tag{25}$$

and E_1 is the solution of

$$R_Z(E_1) = R_Z(E_1+\epsilon) - a \tag{26}$$

In the event that $R_Z(\epsilon) < 2a$, then

$$\left.\frac{df_z}{dE}\right|_{E'=E+\epsilon} = \frac{A\sigma_z\phi}{2S_z(E)} \left\{ \begin{array}{cc} \frac{a^2}{R_Z^2(\epsilon)} + \left[1 - \frac{a^2}{R_Z^2(\epsilon)}\right] \frac{R_Z(E)}{R_Z(E_1)} & (0 \le E \le E_1) \\ 1 & (E_1 \le E \le \infty) \end{array} \right\} \tag{27}$$

with the understanding that E_1 is zero if $R_Z(\epsilon) < a$. The second term of equation (23) is divided into three subintervals as follows:

$$I_1(\epsilon) = \int_{0}^{E_2} \left.\frac{df_z}{d\epsilon}\right|_{E'=E+\epsilon} \rho(E+\epsilon)\, dE \tag{28}$$

$$I_2(\epsilon) = \int_{E_2}^{E_1} \left.\frac{df_z}{d\epsilon}\right|_{E'=E+\epsilon} \rho(E+\epsilon)\, dE \tag{29}$$

$$I_3(\epsilon) = \int_{E_1}^{\infty} \left.\frac{df_z}{d\epsilon}\right|_{E'=E+\epsilon} \rho(E+\epsilon)\, dE \tag{30}$$

First, $I_1(\epsilon)$ is zero unless $R_Z(\epsilon) > 2a$, for which

$$I_1(\epsilon) = \frac{A\sigma_z\phi}{2}\left\{\frac{a^2}{R_Z^2(\epsilon)}P(E_2,\epsilon) + \left[\frac{1}{4} - \frac{a^2}{R_Z^2(\epsilon)}\right]\frac{Q(E_2,\epsilon)}{R_Z(E_2)}\right\} \tag{31}$$

$$I_2(\epsilon) = \frac{A\sigma_z\phi}{2}\left\{\frac{1}{4} - \frac{3}{4}\frac{R_Z(E_2)}{[R_Z(E_1) - R_Z(E_2)]}\right\}[P(E_1,\epsilon) - P(E_2,\epsilon)]$$
$$+ \frac{A\sigma_z\phi}{2}\frac{3}{4}\frac{Q(E_1,\epsilon) - Q(E_2,\epsilon)}{[R_Z(E_1) - R_Z(E_2)]} \tag{32}$$

$$I_3(\epsilon) = \frac{A\sigma_z\phi}{2}\int_{E_1}^{\infty}\frac{\rho(E+\epsilon)}{S_z(E)}\,dE \tag{33}$$

If $a \leq R_Z(\epsilon) \leq 2a$, then E_2 and $I_1(\epsilon)$ are zero and

$$I_2(\epsilon) = \frac{A\sigma_z\phi}{2}\left\{\frac{a^2}{R_Z^2(\epsilon)}P(E_1,\epsilon) + \left[1 - \frac{a^2}{R_Z^2(\epsilon)}\right]\frac{Q(E_1,\epsilon)}{R_Z(E_1)}\right\} \tag{34}$$

When $R_Z(\epsilon) \leq a$, then $E_1 = E_2 = 0$, so that $I_1(\epsilon)$ and $I_2(\epsilon)$ both vanish and

$$I_3(\epsilon) = \frac{A\sigma_z\phi}{2}\int_{0}^{\infty}\frac{\rho(E+\epsilon)}{S_z(E)}\,dE \tag{35}$$

In equations (31), (32), and (34), P and Q are given by

$$P(E_i,\epsilon) = \int_0^{E_i}\frac{\rho(E+\epsilon)}{S_z(E)}\,dE \tag{36}$$

$$Q(E_i,\epsilon) = \int_0^{E_i}\frac{R_Z(E)\rho(E+\epsilon)}{S_z(E)}\,dE \tag{37}$$

The integral of equation (36) may be approximated for values of $E_i \leq \frac{1}{4}\epsilon$ by

$$P(E_i,\epsilon) \approx \frac{R_Z(E_O)}{\sqrt{2}}\rho(\epsilon)\gamma\left(\frac{1}{2},\frac{E_i}{2E_O}\right) \tag{38}$$

where γ is an incomplete gamma function (ref. 23). For larger values of E_i $\left(\frac{1}{4}\epsilon \leq E_i \leq 4\epsilon\right)$, the integral may be taken as

$$P(E_i,\epsilon) \approx \frac{R_Z(E_O)}{\sqrt{2}}\rho(\epsilon)\left\{\frac{1}{2}\gamma\left(\frac{1}{2},\frac{\epsilon}{8E_O}\right) + \frac{1}{2}\gamma\left(\frac{1}{2},\frac{E_i}{2E_O}\right)\right.$$
$$\left. + \sqrt{\frac{2E_O}{\epsilon}}\gamma\left(1,\frac{E_i}{2E_O}\right) - \sqrt{\frac{2E_O}{\epsilon}}\gamma\left(1,\frac{\epsilon}{8E_O}\right)\right\} \tag{39}$$

Whenever $E_i > 4\epsilon$, the integral is approximately

$$P(E_i,\epsilon) \approx \frac{R_Z(E_O)}{\sqrt{2}}\rho(\epsilon)\left\{\frac{1}{2}\gamma\left(\frac{1}{2},\frac{\epsilon}{8E_O}\right) + \frac{1}{2}\gamma\left(\frac{1}{2},\frac{4\epsilon}{2E_O}\right)\right.$$
$$\left. + \sqrt{\frac{2E_O}{\epsilon}}\gamma\left(1,\frac{E_i}{2E_O}\right) - \sqrt{\frac{2E_O}{\epsilon}}\gamma\left(1,\frac{\epsilon}{8E_O}\right)\right\} \tag{40}$$

The integral in equation (37) may be approximated by

$$Q(E_i, \epsilon) \approx \frac{R_Z^2(E_O)}{2E_O} [C(E_i + \epsilon) - C(\epsilon)] \qquad (41)$$

where $C(\epsilon)$ is the integral spectrum as follows:

$$C(E) = \int_0^E \rho(E')\, dE' \qquad (42)$$

A useful check on the approximations involved is the strict requirement

$$I_1(\epsilon) + I_2(\epsilon) + I_3(\epsilon) \leq \frac{A\sigma_z\phi}{2} \int_0^\infty \frac{\rho(E+\epsilon)}{S_z(E)}\, dE \qquad (43)$$

The total absorption spectrum is then

$$\frac{dF}{d\epsilon} = N_S(\epsilon)\rho(\epsilon) + I_1(\epsilon) + I_2(\epsilon) + I_3(\epsilon) \qquad (44)$$

and is shown in figure 7 for detector thicknesses of 1 to 5 μm with $E_O = 3.5$ MeV. Similar results are shown in figure 8 for detector thicknesses of 50 to 200 μm. In comparing figures 8 and 9, it is shown that the energy-loss spectrum is approaching the fragment-production spectrum as a becomes larger. The normalization is always

$$\int_0^\infty \frac{dF}{d\epsilon} = 1 \qquad (45)$$

which is satisfied by numerical evaluation to within 2 percent.

Results

Typical fragmentation cross sections calculated using the Silberberg-Tsao model are shown in table 1 for 125-MeV protons. The values of E_O are taken from reference 14. The calculated response of the 2.5-μm detector is shown in figure 10; these values should be compared with the experiments of McNulty and the values according to the Monte Carlo code of the McNulty group, which are also shown in figure 10. The peak value at zero energy is fixed by the total reaction cross section and total proton flux. It appears that the total reaction cross section of the McNulty code is too small. Otherwise, the present theory and the Monte Carlo code show nearly equivalent agreement with the experiments. Similar comments apply to the 4.2-μm detector response (fig. 11) with one exception. The energetic events above 20 MeV observed in experiments are well represented by the present theory but not by the Monte Carlo code as expected by observing figure 6. This high-energy agreement between theory and experiment is observed for the 24.1-μm detector, but the Monte Carlo code again fails to predict the high-energy events as shown in figure 12. The improved model of the present work is again clearly displayed for the 158-MeV experiments of McNulty et al. as shown in figures 13 and 14.

The inability of the Monte Carlo code to predict the most energetic fragments could be a serious limitation in predicting SEU in some devices. Although the Silberberg-Tsao cross sections for proton-induced reactions are not in complete agreement with some recent cross-section measurements, they still provide improved ability over Monte Carlo models. The methods of analysis used in this paper will be applied to specific-device geometries in the near future.

Concluding Remarks

Although the intranuclear-cascade code provides a very detailed model of the nuclear reactions of high-energy protons, the inaccuracies of current cascade and compound nuclear-decay models limit the usefulness of such models in single-event upset studies. The improved predictions of the current semi-empirical cross sections of the Silberberg-Tsao model seem adequate for microelectronic studies.

NASA Langley Research Center
Hampton, VA 23665-5225
September 7, 1989

References

1. Binder, D.; Smith, E. C.; and Holman, A. B.: Satellite Anomalies From Galactic Cosmic Rays. *IEEE Trans. Nucl. Sci.*, vol. NS-22, no. 6, Dec. 1975, pp. 2675–2680.
2. Wyatt, R. C.; McNulty, P. J.; Toumbas, P.; Rothwell, P. L.; and Filz, R. C.: Soft Errors Induced by Energetic Protons. *IEEE Trans. Nucl. Sci.*, vol. NS-26, no. 6, Dec. 1979, pp. 4905–4910.
3. Guenzer, C. S.; Allen, R. G.; Campbell, A. B.; Kidd, J. M.; Petersen, E. L.; Seeman, N.; and Wolicki, E. A.: Single Event Upsets in RAMs Induced by Protons at 4.2 GeV and Protons and Neutrons Below 100 MeV. *IEEE Trans. Nucl. Sci.*, vol. NS-27, no. 6, Dec. 1980, pp. 1485–1489.
4. Petersen, E. L.: Nuclear Reactions in Semiconductors. *IEEE Trans. Nucl. Sci.*, vol. NS-27, no. 6, Dec. 1980, pp. 1494–1499.
5. McNulty, P. J.; Farrell, G. E.; Wyatt, R. C.; Rothwell, P. L.; Filz, R. C.; and Bradford, J. N.: Upset Phenomena Induced by Energetic Protons and Electrons. *IEEE Trans. Nucl. Sci.*, vol. NS-27, no. 6, Dec. 1980, pp. 1516–1522.
6. McNulty, Peter J.; Farrell, Gary E.; and Tucker, William P.: Proton-Induced Nuclear Reactions in

Silicon. *IEEE Trans. Nucl. Sci.,* vol. NS-28, no. 6, Dec. 1981, pp. 4007–4012.

7. Hamm, R. N.; Rustgi, M. L.; Wright, H. A.; and Turner, J. E.: Energy Spectra of Heavy Fragments From the Interaction of Protons With Communications Materials. *IEEE Trans. Nucl. Sci.,* vol. NS-28, no. 6, Dec. 1981, pp. 4004–4006.
8. Bradford, John N.: Microvolume Energy Deposition From High Energy Proton-Silicon Reactions. *IEEE Trans. Nucl. Sci.,* vol. NS-29, no. 6, Dec. 1982, pp. 2085–2089.
9. Bisgrove, J. M.; Lynch, J. E.; McNulty, P. J.; Abdel-Kader, W. G.; Kletnieks, V.; and Kolasinski, W. A.: Comparison of Soft Errors Induced by Heavy Ions and Protons. *IEEE Trans. Nucl. Sci.,* vol. NS-33, no. 6, Dec. 1986, pp. 1571–1576.
10. Fernald, Kenneth W.; and Kerns, Sherra E.: Simulation of Proton-Induced Energy Deposition in Integrated Circuits. *IEEE Trans. Nucl. Sci.,* vol. NS-35, no. 1, Feb. 1988, pp. 981–986.
11. Petersen, E. L.; Shapiro, P.; Adams, J. H., Jr.; and Burke, E. A.: Calculation of Cosmic-Ray Induced Soft Upsets and Scaling of VLSI Devices. *IEEE Trans. Nucl. Sci.,* vol. NS-29, no. 6, Dec. 1982, pp. 2055–2063.
12. Tsao, C. H.; Silberberg, R.; Adams, J. H., Jr.; and Letaw, J. R.: Cosmic Ray Transport in the Atmosphere—Dose and LET-Distributions in Materials. *IEEE Trans. Nucl. Sci.,* vol. NS-30, Dec. 1983, pp. 4398–4404.
13. Wilson, John W.; Townsend, L. W.; Chun, S. Y.; and Buck, W. W.: High Energy Nucleon Data Bases. *Health Phys.,* vol. 55, Nov. 1988, pp. 817–819.
14. Wilson, John W.; Townsend, Lawrence W.; Nealy, John E.; Chun, Sang Y.; Hong, B. S.; Buck, Warren W.; Lamkin, S. L.; Ganapol, Barry D.; Khan, Ferdous; and Cucinotta, Francis A.: *BRYNTRN: A Baryon Transport Model.* NASA TP-2887, 1989.
15. Chern, J. H.; Seitchik, J. A.; and Yang, P.: Single Event Charge Collection Modeling in CMOS Multijunctions Structure. *1986 International Electron Devices Meeting—Technical Digest,* IEEE Catalog No. 86CH2381-2, Inst. of Electrical and Electronics Engineers, Inc., c.1986, pp. 538–541.
16. Rudstam, G.: Systematics of Spallation Yields. *Zeitschrift fur Naturforschung,* vol. 21a, no. 7, July 1966, pp. 1027–1041.
17. Serber, R.: Nuclear Reactions at High Energies. *Phys. Review,* vol. 72, no. 11, Dec. 1, 1947, pp. 1114–1115.
18. Bertini, Hugo W.: Intranuclear-Cascade Calculation of the Secondary Nucleon Spectra From Nucleon-Nucleus Interactions in the Energy Range 340 to 2900 MeV and Comparisons With Experiment. *Phys. Review,* second ser., vol. 188, no. 4, Dec. 20, 1969, pp. 1711–1730.
19. Kwiatkowski, K.; Zhou, S. H.; Ward, T. E.; Viola, V. E., Jr.; Brever, H.; Mathews, G. J.; Gökmen, A.; and Mignerey, A. C.: Energy Deposition in Intermediate-Energy Nucleon-Nucleus Collisions. *Phys. Review Lett.,* vol. 50, no. 21, May 23, 1983, pp. 1648–1651.
20. Wilson, John W.; and Lamkin, Stanley L.: Perturbation Theory for Charged-Particle Transport in One Dimension. *Nucl. Sci. & Eng.,* vol. 57, no. 4, Aug. 1975, pp. 292–299.
21. Wilson, John W.: *Analysis of the Theory of High-Energy Ion Transport.* NASA TN D-8381, 1977.
22. Goldhaber, A. S.: Statistical Models of Fragmentation Processes. *Phys. Lett.,* vol. 53B, no. 4, Dec. 23, 1974, pp. 306–308.
23. Abramowitz, Milton; and Stegun, Irene A., eds.: *Handbook of Mathematical Functions With Formulas, Graphs, and Mathematical Tables.* NBS Appl. Math. Ser. 55, U.S. Dep. of Commerce, June 1964.

Table 1. Cross-Section Parameters for Fragmentation of ^{28}Si by 125-MeV Protons

A_F	σ_F, mb	E_O, MeV
27	67.7	0.17
26	50.8	.34
25	44.5	.50
24	37.7	.67
23	24.7	.84
22	24.5	1.01
21	14.7	1.17
20	15.3	1.34
19	8.1	1.51
18	7.3	1.68
17	6.4	1.85
16	6.1	2.01
15	4.2	2.18
14	2.9	2.35
13	1.9	2.52
12	2.3	2.68
11	1.5	2.85
10	1.0	3.02
9	1.1	3.19
8	1.7	3.35
7	1.9	3.52
6	1.5	3.69
5	1.2	3.86
4	145.9	2.08
3	29.1	2.92
2	70.7	2.06
1	710.5	2.06

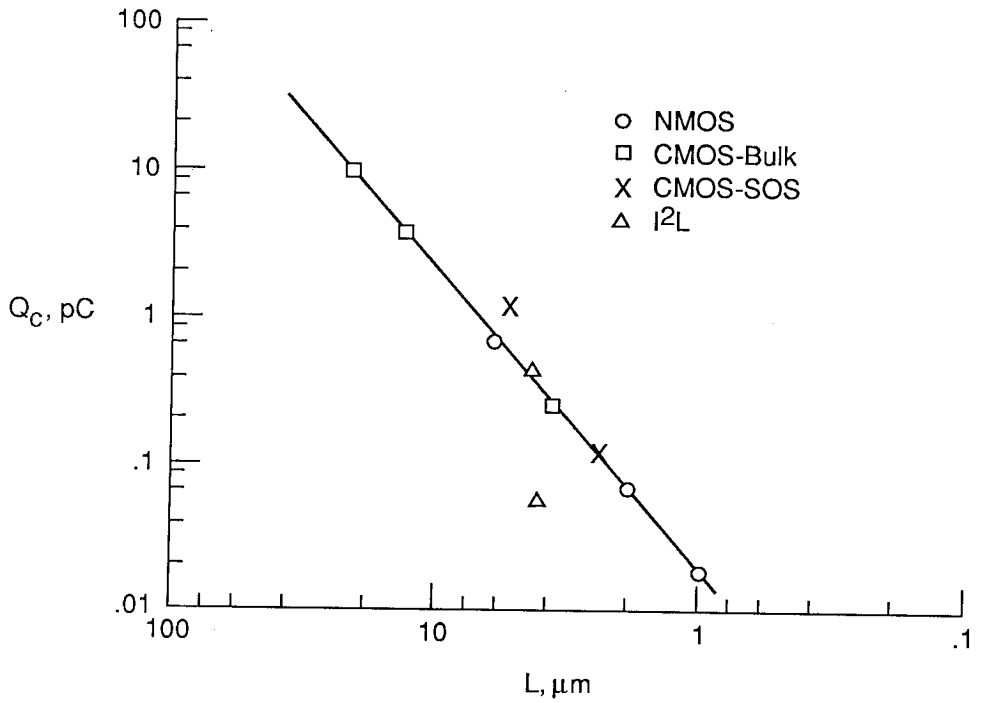

Figure 1. Critical charge as a function of feature size in several device types.

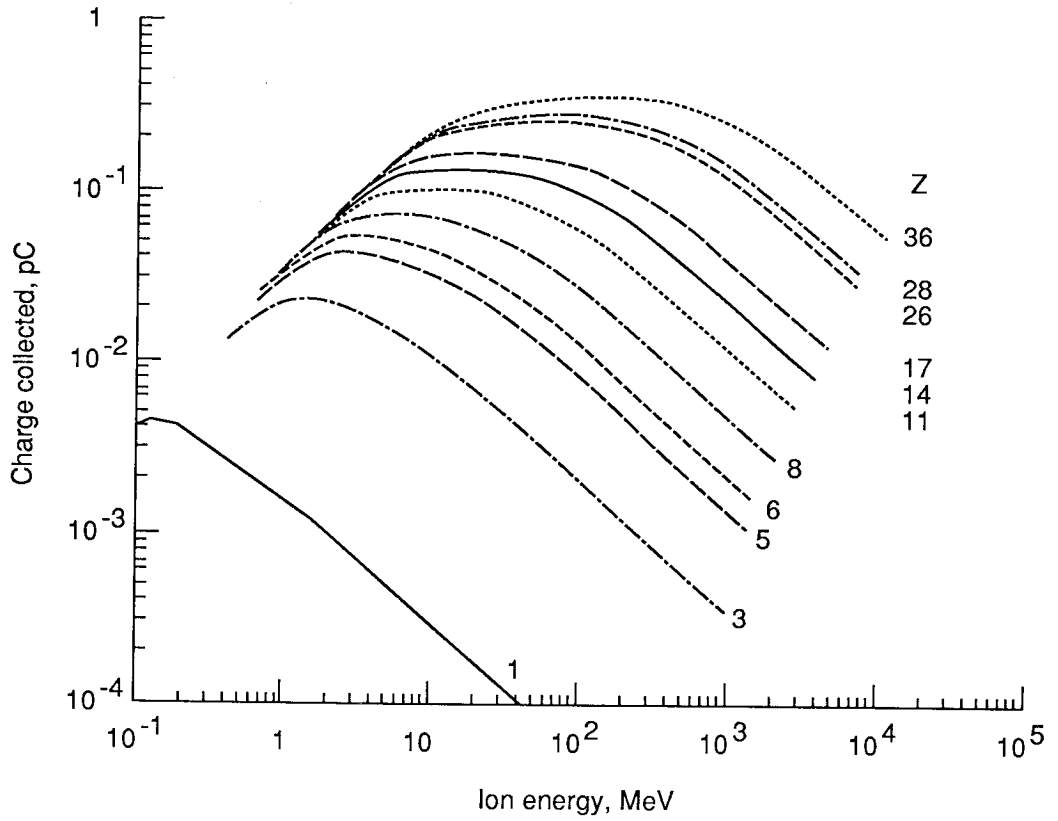

Figure 2. Charge collected as a function of ion energy with a collection length of 2 μm.

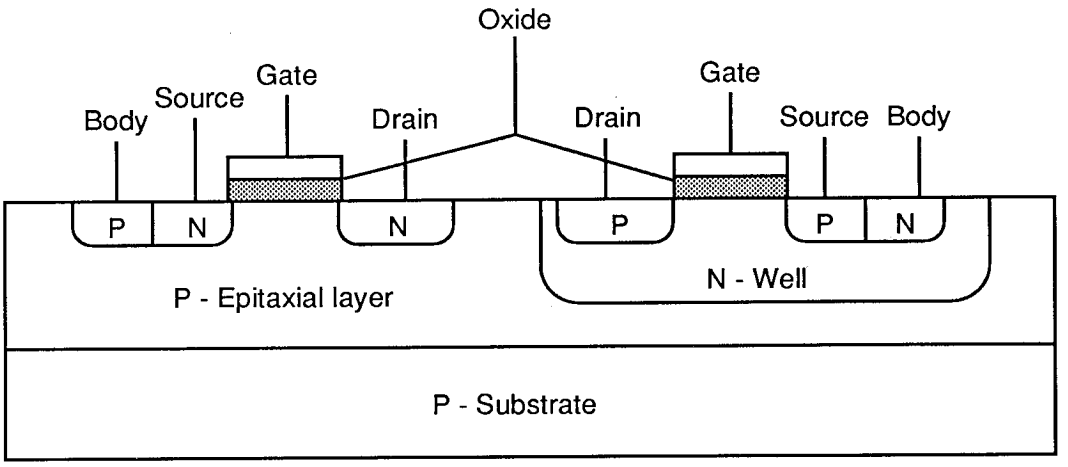

Figure 3. Cross section of bulk CMOS technology.

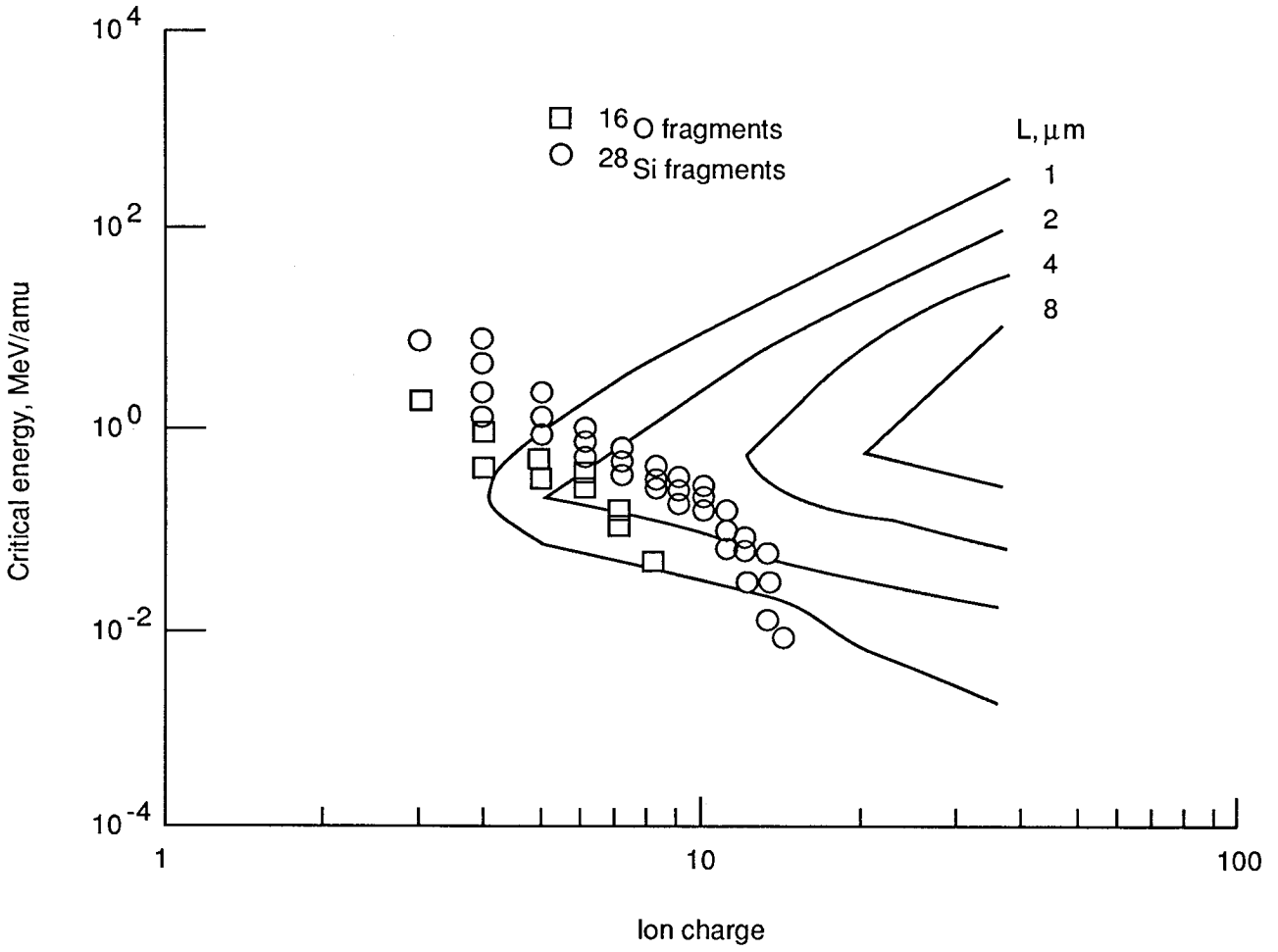

Figure 4. Critical energy as a function of ion charge for several feature sizes. Average recoil energies of fragments of silicon and oxygen are superimposed.

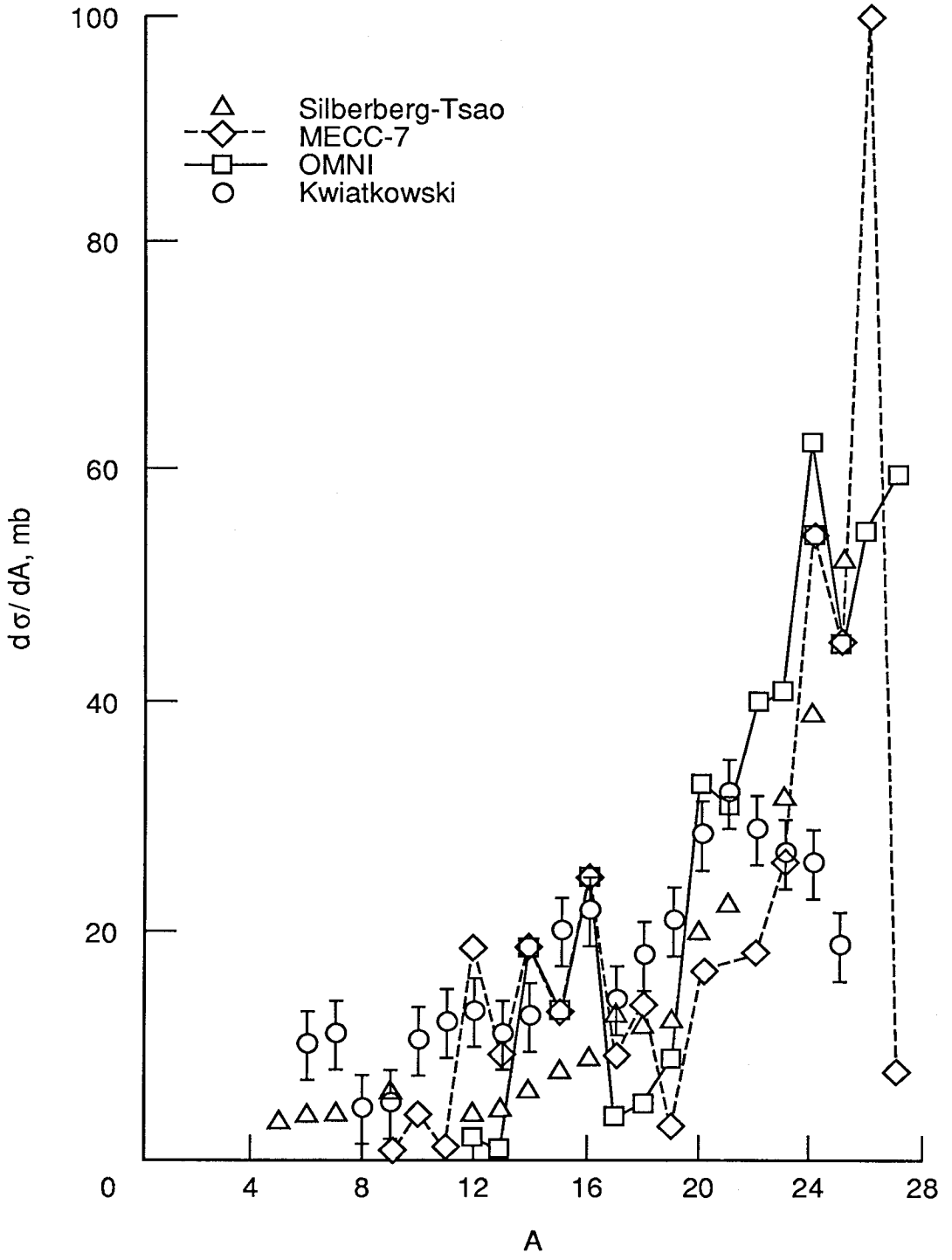

Figure 5. Fragmentation cross section for 180-MeV protons on Al targets calculated by various models compared with experimental measurements.

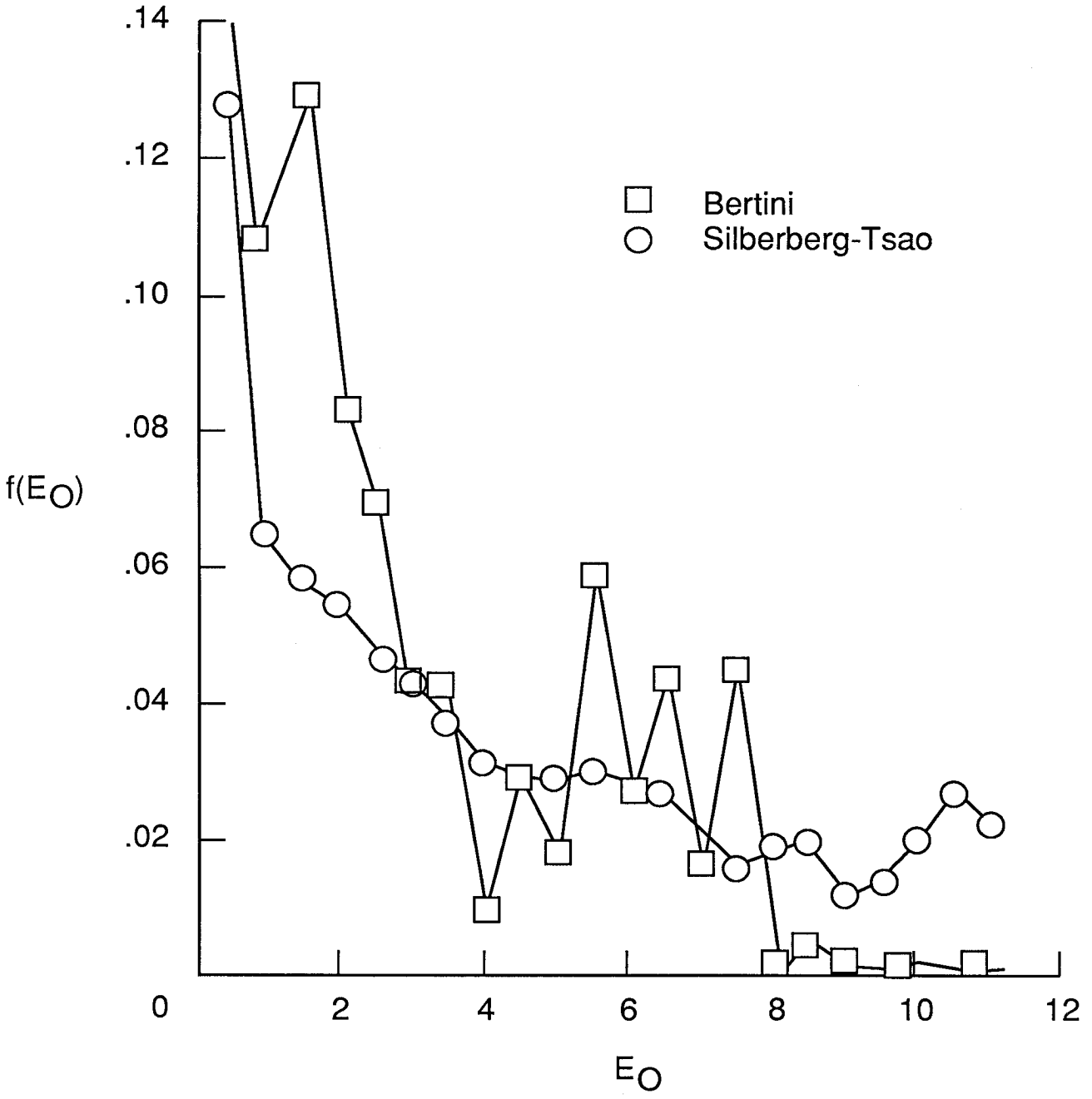

Figure 6. Spectrum of average energy predicted by Silberberg and Tsao cross sections compared with Bertini cross sections.

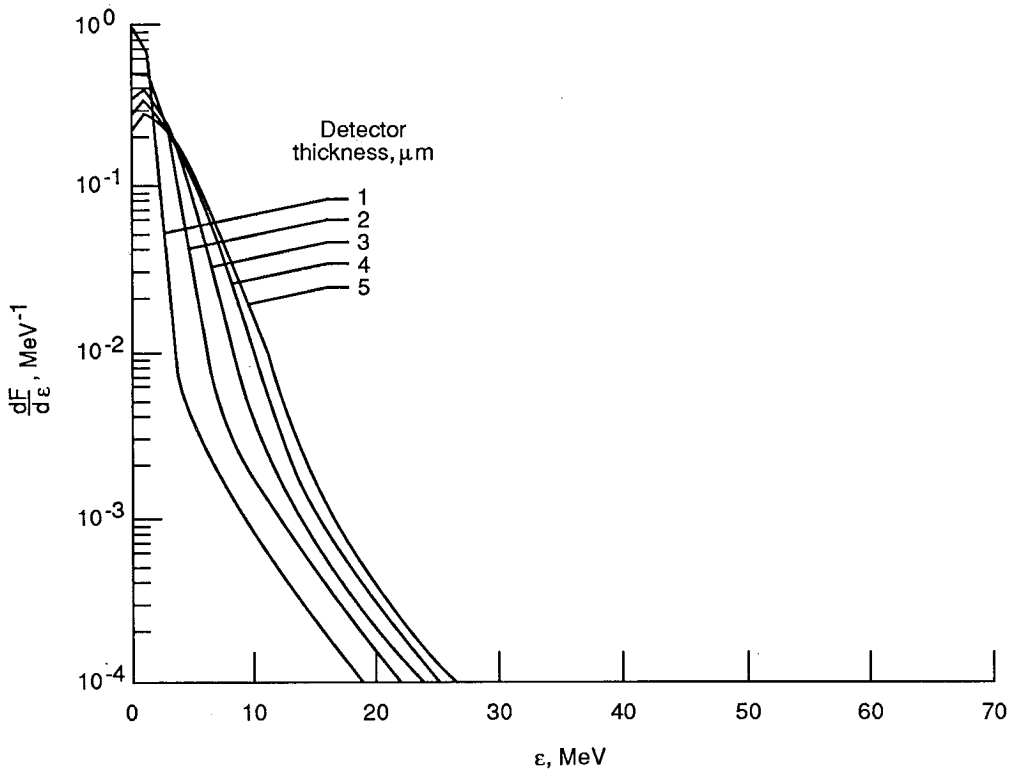

Figure 7. Total absorption spectrum for surface-barrier detector of 1 to 5 μm and $E_O = 3.5$ MeV.

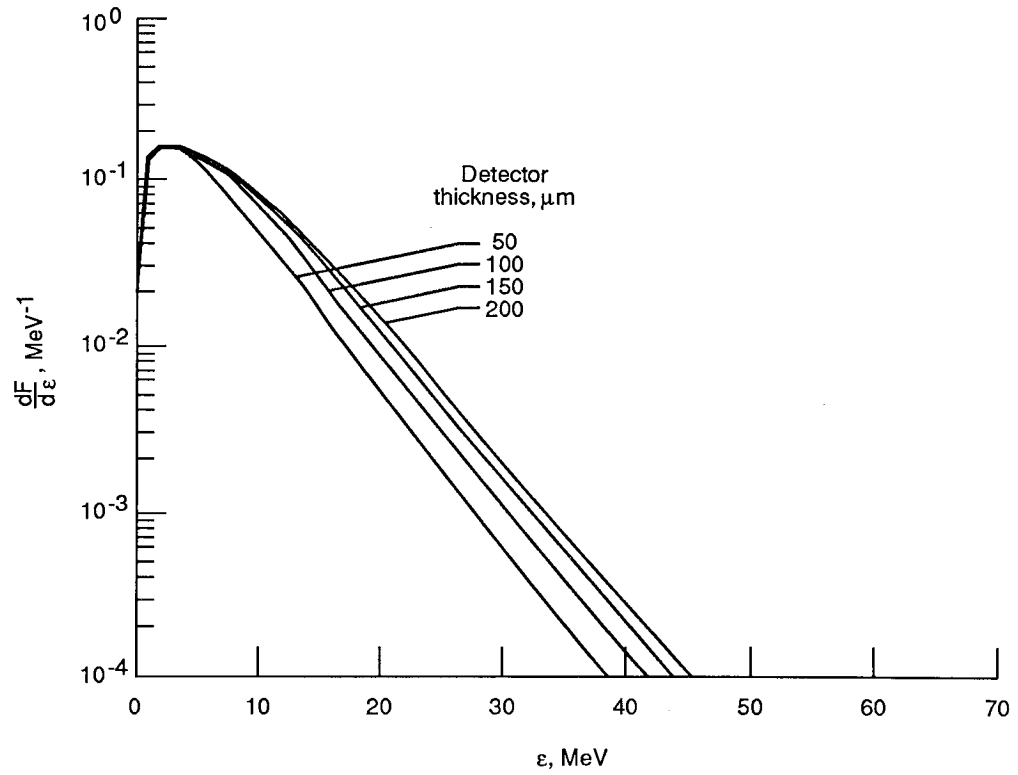

Figure 8. Total absorption spectrum for surface-barrier detector of 50 to 200 μm and $E_O = 3.5$ MeV.

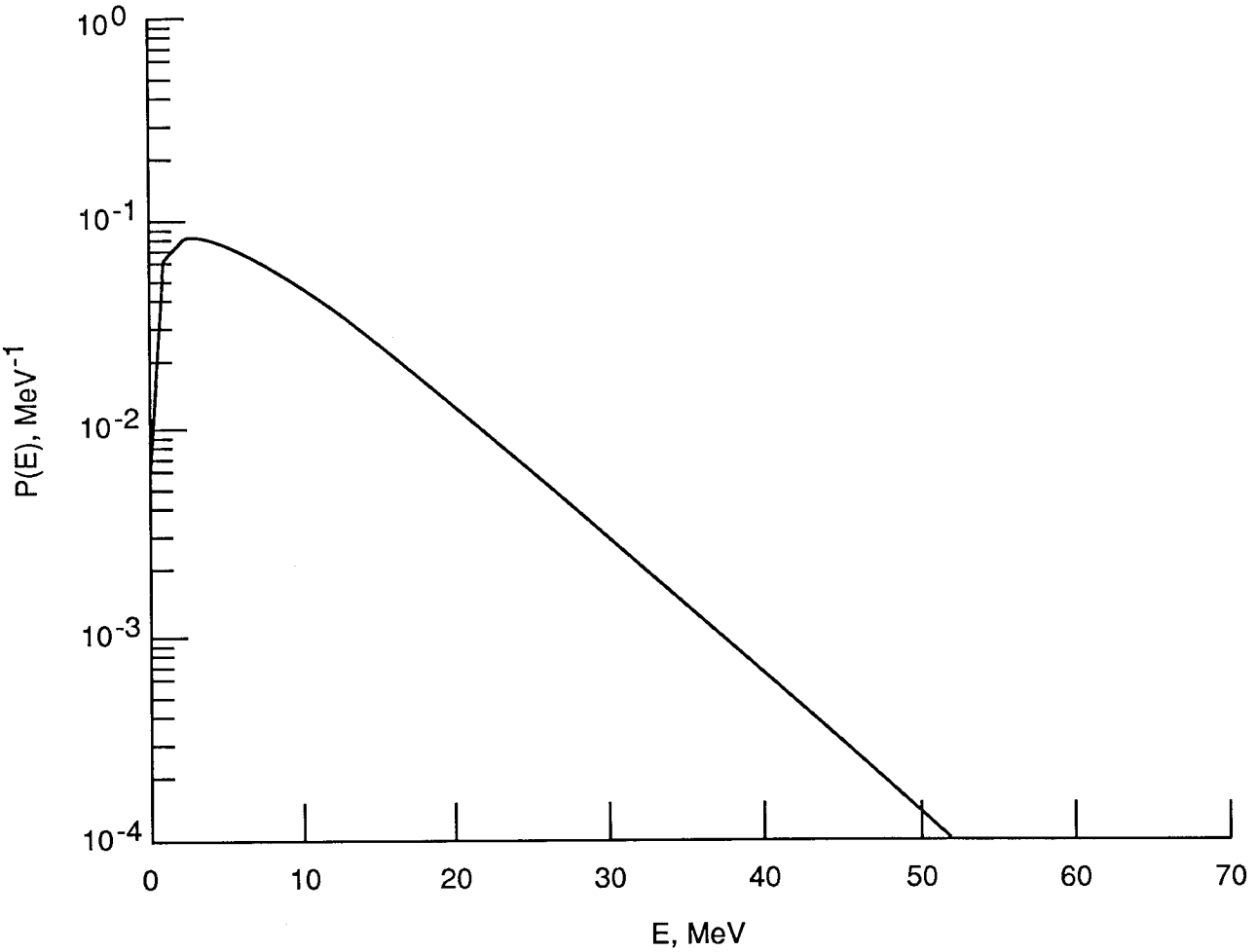

Figure 9. Energy-loss spectrum for $E_O = 3.5$ MeV.

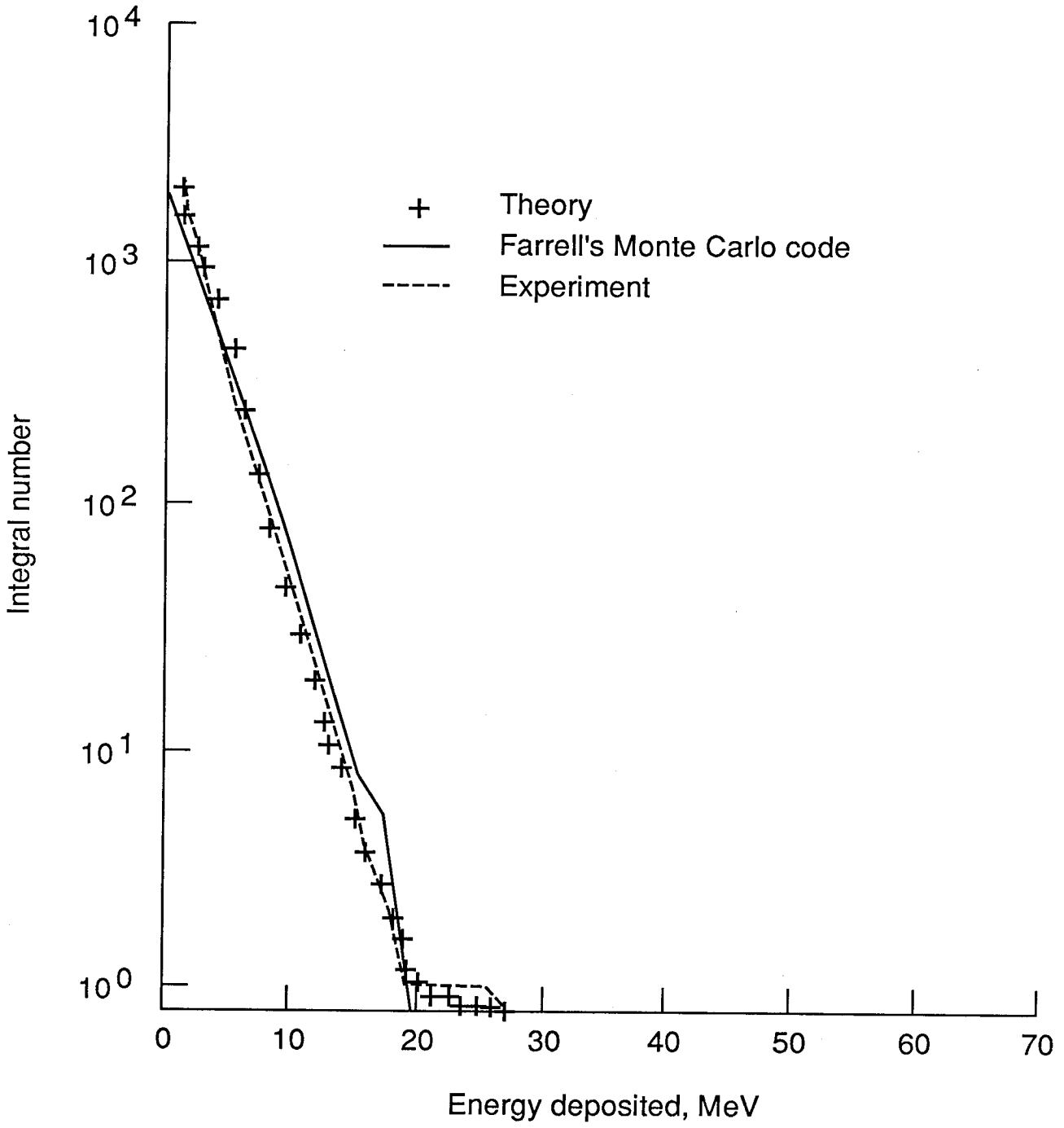

Figure 10. Response of a 2.5-μm surface-barrier detector to 125-MeV protons (2.14×10^8 protons).

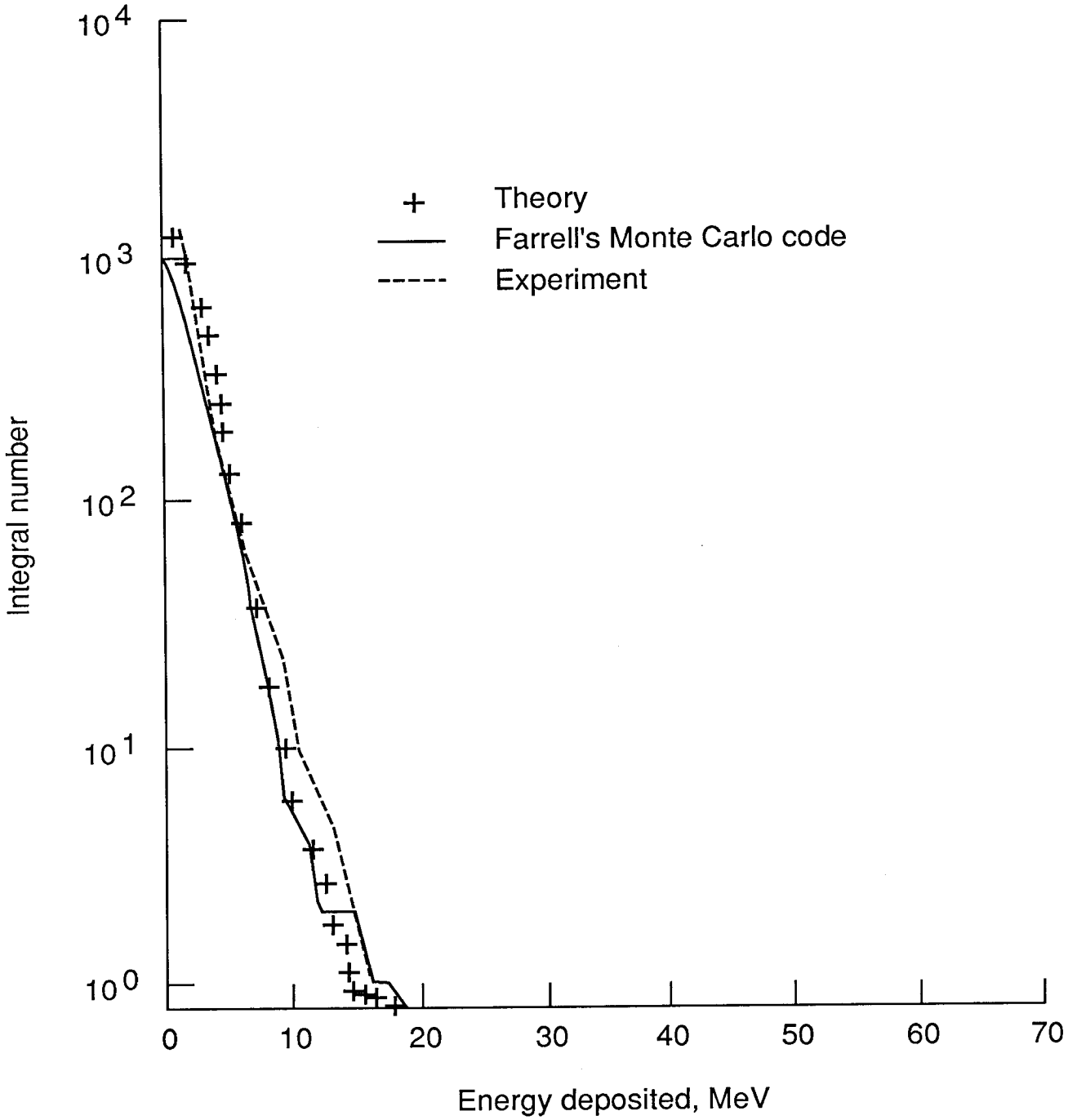

Figure 11. Response of a 4.2-μm surface-barrier detector to 125-MeV protons (2.14×10^8 protons).

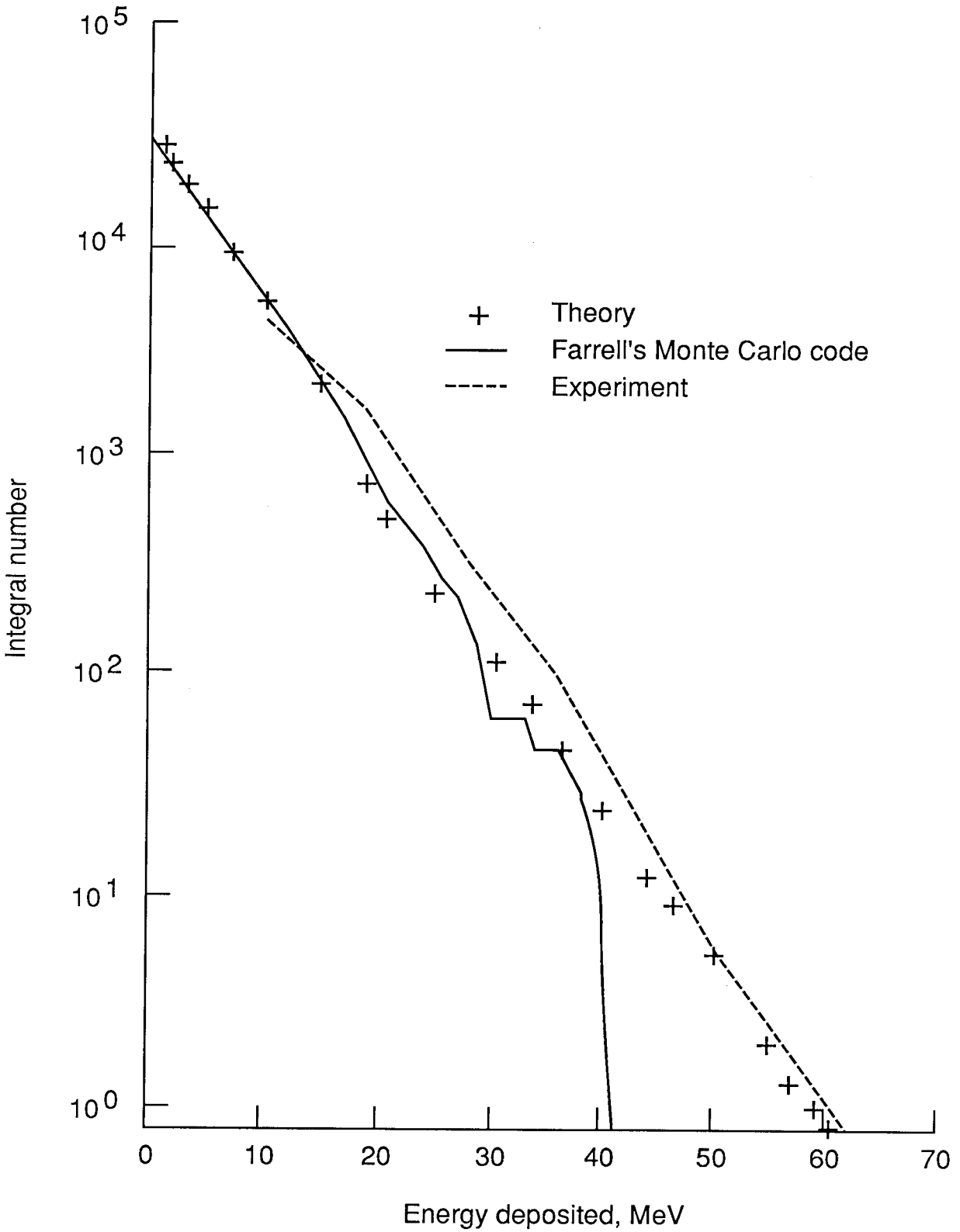

Figure 12. Response of a 24.1-μm surface-barrier detector to 125-MeV protons (6.42×10^8 protons).

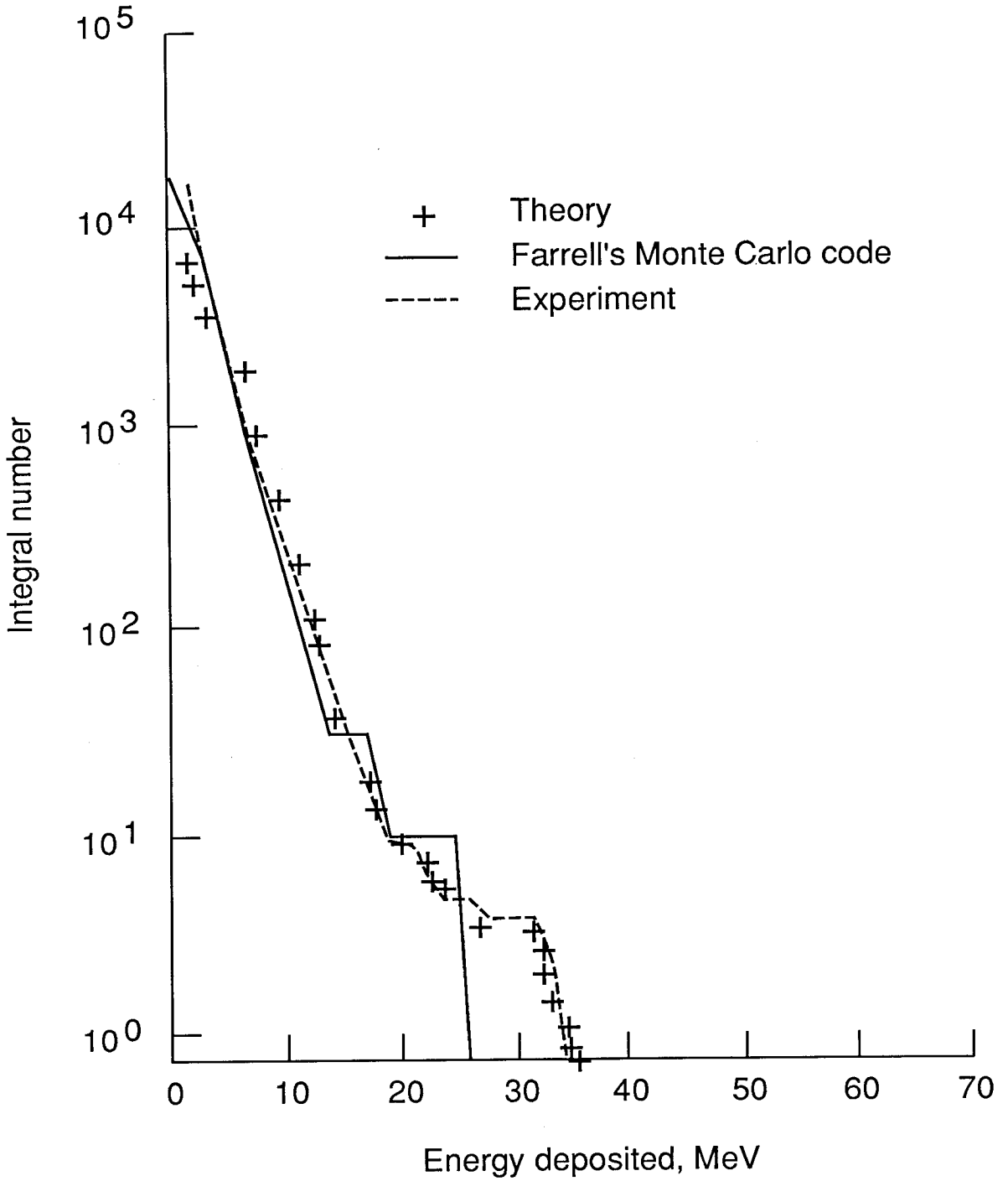

Figure 13. Response of a 2.5-μm surface-barrier detector to 158-MeV protons (3.9×10^9 protons).

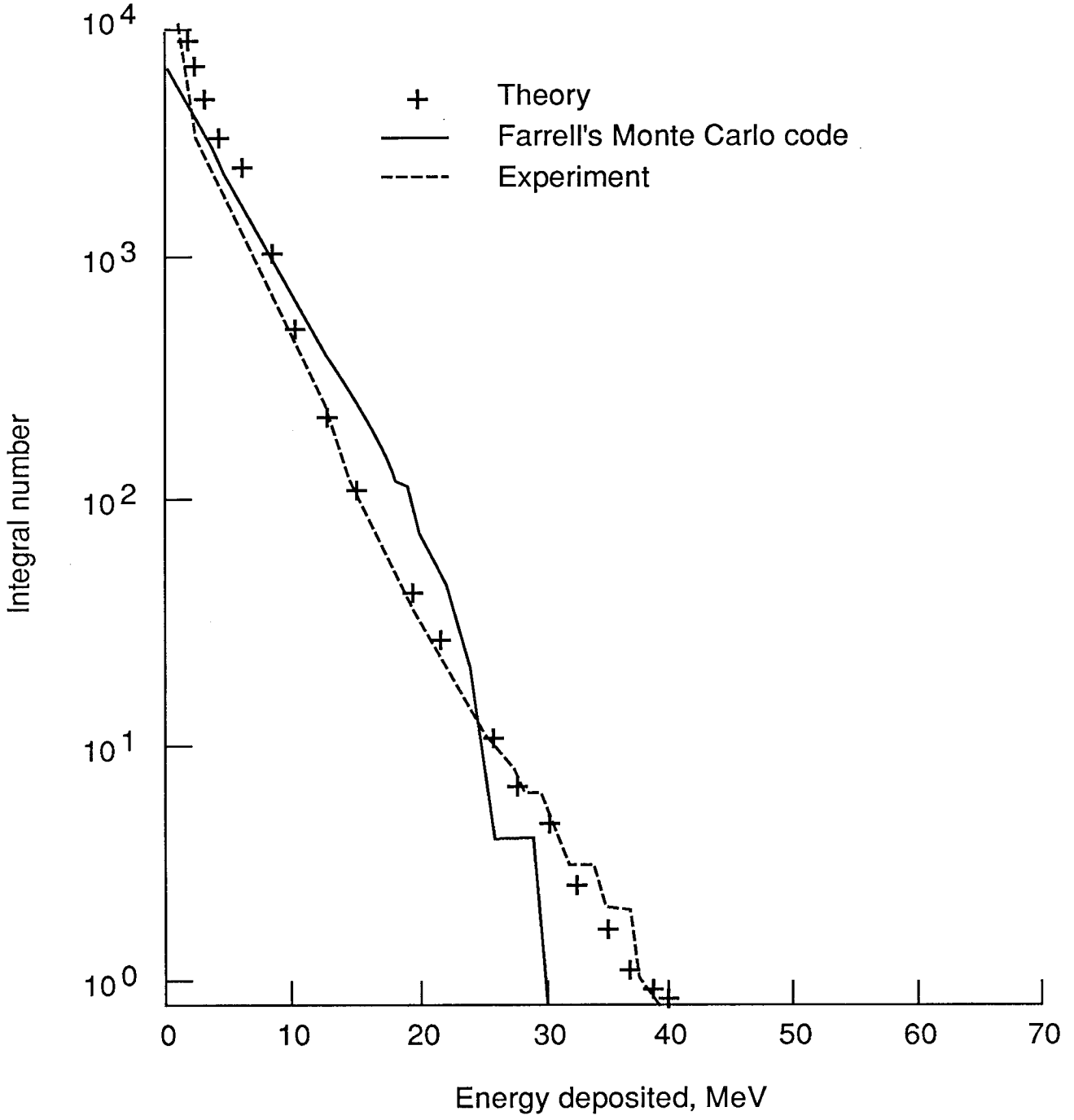

Figure 14. Response of an 8.7-μm surface-barrier detector to 158-MeV protons (3.9×10^8 protons).

NASA
National Aeronautics and Space Administration

Report Documentation Page

1. Report No.	2. Government Accession No.	3. Recipient's Catalog No.
NASA TM-4143		

4. Title and Subtitle	5. Report Date
Nuclear-Fragmentation Studies for Microelectronic Applications	November 1989
	6. Performing Organization Code

7. Author(s)	8. Performing Organization Report No.
Duc M. Ngo, John W. Wilson, Warren W. Buck, and Thomas N. Fogarty	L-16635
	10. Work Unit No.
9. Performing Organization Name and Address	584-02-11-01
NASA Langley Research Center Hampton, VA 23665-5225	11. Contract or Grant No.

12. Sponsoring Agency Name and Address	13. Type of Report and Period Covered
National Aeronautics and Space Administration Washington, DC 20546-0001	Technical Memorandum
	14. Sponsoring Agency Code

15. Supplementary Notes

Duc M. Ngo, Warren W. Buck, and Thomas N. Fogarty: Hampton University, Hampton, Virginia.
John W. Wilson: Langley Research Center, Hampton, Virginia.

16. Abstract

A formalism for target fragment transport is presented with application to energy-loss spectra in thin silicon devices. Predicted results are compared with experiments using the surface-barrier detectors developed by J. P. McNulty. The intranuclear-cascade, nuclear-reaction model does not predict the McNulty experimental data for the highest energy events. A semiempirical nuclear cross section gives an adequate explanation of McNulty's experiments. Application of the formalism to specific electronic devices is discussed.

17. Key Words (Suggested by Authors(s))	18. Distribution Statement
Low-energy transport Data bases Neutron-nucleus Cross sections Electronics	Unclassified–Unlimited Subject Category 93

19. Security Classif. (of this report)	20. Security Classif. (of this page)	21. No. of Pages	22. Price
Unclassified	Unclassified	21	A03

For sale by the National Technical Information Service, Springfield, Virginia 22161-2171